Nanoscale and Microscale Thermophysical Engineering, 19: 245–257, 2015

ISSN: 1556-7265 print / 1556-7273 online
DOI: 10.1080/15567265.2015.1078425

ASSESSMENT OF THERMAL PROPERTIES VIA NANOSECOND THERMOREFLECTANCE METHOD

Richard Garrelts[1,2], Amy Marconnet[2,3], and Xianfan Xu[2,3]

[1]*Department of Physics and Astronomy, Purdue University, West Lafayette, Indiana, USA*
[2]*Birck Nanotechnology Center, Purdue University, West Lafayette, Indiana, USA*
[3]*School of Mechanical Engineering, Purdue University, West Lafayette, Indiana, USA*

Nanosecond time-domain thermoreflectance (ns-TDTR) is an all optical method of determining independently a variety of thermal parameters of both homogeneous and layered materials. Despite its relative experimental simplicity, the sensitivity of the temperature decay (measured by the transient reflectivity signal) to the relevant thermal properties has yet to be fully characterized. In principle, it is possible to simultaneously extract multiple thermal parameters from a single measurement. In practice, however, changes to several of these parameters may result in experimentally indistinguishable variations to the transient reflectivity signal. In this work, we focus on investigating thermal properties of bulk material and the contact resistance between the thin-film coating that is needed for the ns-TDTR method and the bulk substrate. To extract multiple properties from one temperature decay trace, we divide the data into temporal sub-regions known to be influenced to different degrees by each individual thermal parameter and iteratively fit with a 1-D heat conduction model to independently determine the contact resistance and cross-plane thermal conductivity.

KEY WORDS: ns Thermoreflectance, thermal contact resistance, thermal conductivity

INTRODUCTION

Interfacial and bulk thermal transport properties are of primary concern in all scales of device design. Thermal energy transfer through micro and nanoscale devices may be dominated by either intra-layer or interfacial transport properties [1], and independent characterization of these properties can be particularly challenging. Several methods have been developed for measuring thermal transport properties, each possessing their own limitations. Broadly speaking, thermal property measurement techniques can be divided into contact and non-contact methods, as well as steady-state and transient methods. Contact methods typically involve incorporating the sample of interest into an electronic circuit, the temperature-dependent behavior of which is assessed and subsequently related to an unknown thermal property of the sample through appropriate modeling. Techniques in this category include the 3ω method [2], bolometry [3], and electrical pulse heating [4].

Manuscript received 23 April 2015; accepted 27 July 2015.

Address correspondence to Xianfan Xu, Birck Nanotechnology Center, Purdue University, West Lafayette, Indiana 47907, USA. E-mail: xxu@ecn.purdue.edu

Color versions of one or more of the figures in the article can be found online at www.tandfonline.com/umte

Non-contact techniques, in contrast, involve measurement of some temperature-dependent property that does not require sample incorporation into an electric circuit. Raman thermometry [5, 6], the photo-acoustic method [7], time-domain thermoreflectance (TDTR) [8], dilatometry [9], and the laser flash method [10] are the most commonly used non-contact techniques. The relative simplicity of sample preparation involved in these non-contact techniques and their ability to deal with a variety of sample geometries makes them suitable for many material measurements.

In thermoreflectance measurements, a sample is first coated with a thin metal film, which acts as a temperature transducer layer. The film is transiently heated by a pulsed laser, and a second laser (either pulsed or cw) is used to monitor the change in reflectivity of the metal layer as a function of time [11, 12] or modulation frequency [13,14]. Because reflectivity depends on temperature, this second beam allows contactless assessment of changes in the temperature of the metal surface layer. Following the transient heating pulse, the temperature of the surface layer decreases at a rate determined by the thermal properties of the sample. This temperature decay is then used to extract the thermal property of interest through comparison with an appropriate model of heat transfer. While much attention has been paid to ultra-fast thermoreflectance techniques [15-17], using nanosecond laser for thermoreflectance measurement remains less appreciated. TDTR employing nanosecond lasers as a pump allows for the monitoring of surface temperature in real time without the use of either lock-in amplification or complicated delay stage arrangements. Therefore, the setup costs and potential alignment issues are substantially reduced. Moreover, nanosecond pulsed lasers typically have a repetition rate over tens of kHz, allowing for fast averaging over large number of data. Finally, TDTR measurements employing nanonsecond pulse widths do not produce complicated electron-lattice non-equilibrium effects seen in femtosecond TDTR measurements. With proper sample design, nanosecond TDTR can provide accurate measurements of thermal properties with similar sensitivity as ultra-fast TDTR methods.

EXPERIMENT

In order to assess sensitivity of ns-TDTR to substrate conductivity and thermal boundary resistance, transient reflectivity measurements are carried out on bulk Si, GaAs, and glass coated with 100 nm Au as a transducer layer. The sample surface is transiently heated using a frequency doubled (532 nm wavelength) pulsed (4.5 ns pulsewidth) pump Nd:YAG laser system with a 5 kHz repetition rate. The typical average pump power is approximately 100 mW, resulting in approximately 20 μJ per pulse. The resulting change in surface temperature is monitored by a CW He-Ne (633 nm wavelength) probe laser operating at 2.5 mW. In order to reduce the effect of fluctuations in probe laser power, the reflected signal is registered on a two-channel fast photodiode (upper frequency limit 350 MHz) referenced to the probe laser output. The output of the photodiode is fed to an oscilloscope (bandwidth 500 MHz) and scattered pump light reflected from one of the mirrors used to steer the pump beam is employed as a trigger for the oscilloscope. A schematic of the setup and typical measurement result are shown in Figure 1. The change in temperature at the surface of the sample is estimated to be less than 5 °C in all cases, and this has been verified using the time-domain heat transfer model described in the following section. For all measurements, the diameter of the pump laser spot is at least 2 mm while the probe beam diameter is approximately 100 μm to ensure 1D heat transfer in the probed area.

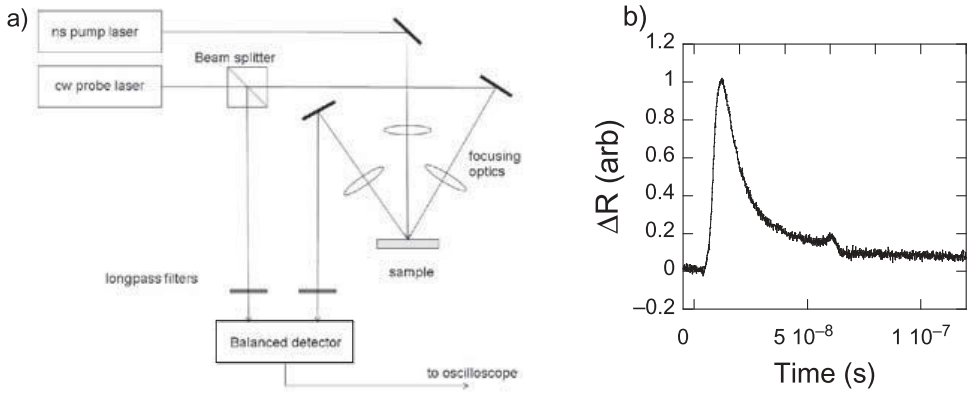

Figure 1 Schematic of the ns thermoreflectance measurement system (a) and typical measurement result (b).

A typical transient reflectivity curve is shown in Figure 1b. The bump in the data at approximately 60 ns is an artifact resulting from a secondary pulse of the pump laser. In order to avoid possible biasing of the best-fit results, this region is removed from the consideration in the least squares data processing algorithm described in the following sections.

HEAT TRANSFER MODELING

Measurements typically employ average pump powers of approximately 100 mW and a beam diameter of ∼2 mm. For a 5 kHz repetition rate of laser pulses ∼5 ns in duration, this implies a peak power of order 10 kW and a peak intensity of order 3 MW/cm^2. This intensity is greater than the CW probe intensity by five orders of magnitude; therefore heating induced by the probe laser can safely be neglected. As the probe is about 100 μm in diameter, much smaller than the ∼2 mm diameter of the pump, and the thermal penetration depth in the time scale of consideration is of the order of μm, the subsequent heat transfer process can be described by a simple set of 1-D diffusion equations [18]. The transient heating induced by the pump laser incident on the sample surface may be modeled by a source term of the form [18]

$$S(x,t) = \frac{.94(1-R_{pump})J}{t_p\alpha_l\left[1-\exp\left(\frac{-L}{\alpha_l}\right)\right]}\exp\left[-2.77\frac{(t-2t_p)^2}{{t_p}^2}-\frac{x}{\alpha_l}\right] \tag{1}$$

where R_{pump} is the sample reflectivity at the pump laser wavelength, J the laser fluence, t_p the pulsewidth of the pump laser, L the thickness of the metal layer, and α_l the optical absorption depth. The constant of 2.77 expands the shape of the exponential to be Gaussian with a full width at half maximum of t_p.

Provided the transducer layer is of sufficient thickness, the pump beam can be assumed to negligibly penetrate any underlying layers, and the resulting transfer of energy through the thickness of the sample is described by

$$\rho_m c_m\left(\frac{\partial T_m}{\partial t}\right) = \frac{\partial}{\partial x}\left(K_m\frac{\partial T_m}{\partial x}\right) + S(x,t) \tag{2}$$

and

$$\rho_s c_s \left(\frac{\partial T_s}{\partial t}\right) = \frac{\partial}{\partial x}\left(k_s \frac{\partial T_s}{\partial x}\right) \tag{3}$$

where ρ is the density of the material, c is the specific heat per unit mass, and k is the thermal conductivity. The subscripts m and s denote the metal layer and substrate, respectively. The boundary conditions are given by

$$-k_m \frac{\partial T_m}{\partial x}\bigg|_{x=L} = -k_s \frac{\partial T_s}{\partial x}\bigg|_{x=L} = \frac{T_m - T_s}{R}\bigg|_{x=L} \tag{4}$$

where R is the interfacial thermal resistance between the metal layer and substrate. This approach may be expanded for samples consisting of arbitrarily many layers by introducing an equation of the form of Eq. (3) for each layer and an equation of the form of Eq. (4) for each interface.

Due to the low temperature rise, ρ, c, k, and R are taken to be independent of temperature. Additionally, the heat loss to the air is assumed to be negligible in comparison to the heat flux provided by the pump laser through the metal layer, and an insulating boundary condition is applied at the metal-air interface. Typically, the substrate is of sufficient thickness to ensure that the temperature at the back surface of the substrate does not measurably increase over the time scales investigated in these experiments, and an insulating boundary condition may, therefore, also be applied at the back sample surface.

The output of the model is subsequently normalized and compared to experiment. Provided that the change in temperature of the metal surface layer is sufficiently small, the refractive index of the layer can be considered to vary linearly with temperature. Thus, monitoring the change in reflectivity of the metal layer as a function of time is equivalent to monitoring the normalized change in temperature of the surface of the metal layer. After normalization, the thermal property of interest is treated as a free parameter in the model, and a least squares algorithm is utilized to assess the quality of the fit to a range of possible values.

In principle, only heat capacity and density cannot be disentangled from one another in the modeled results. Because experimental results are always accompanied by noise, however, it may be impossible in practice to determine simultaneously several thermal properties of interest from a single measurement. It is important to carry out numerical calculations prior to measurements to evaluate the measurement sensitivity. As an example, we analyze below the effects of thermal conductivity of the bulk substrate and the interface contact resistance, the two parameters are often of primary interest, as well as the effect of the thickness of the transducer layer.

Sensitivity of the thermoreflectance measurement to a particular parameter of interest is maximized when the parameter of interest dominates the thermal transfer and significantly influences the reflectivity signal. For comparison, Figures 2a and 2b show the calculated dependence of the temperature (reflectivity) change on interfacial resistance for substrate materials with high (Si) and low (glass) thermal conductivities coated with identical thicknesses of Au. Sensitivity of the transient reflectivity signal to contact resistance varies with the bulk thermal properties of the substrate. In the case of Si, the thermal conductivity is sufficiently high that the contact resistance (rather than the substrate thermal properties) largely determines the rate of cooling of the metal transducer layer. In contrast,

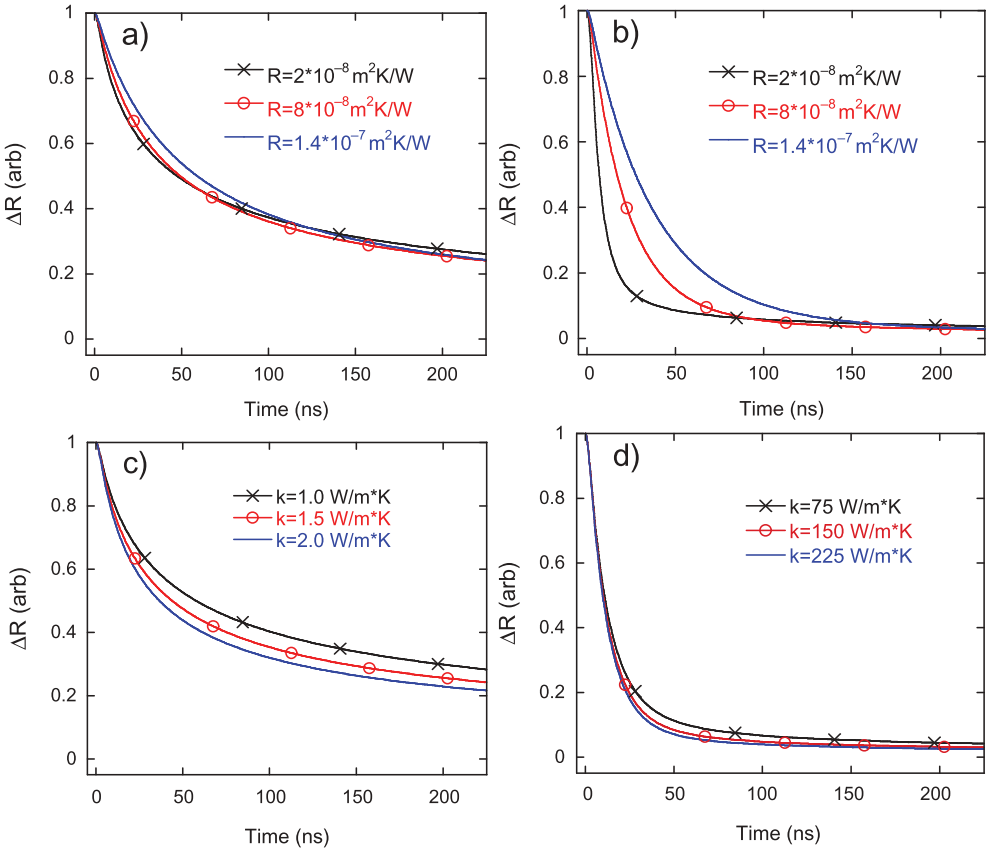

Figure 2 Comparison of TDTR sensitivity to interfacial contact resistance for (a) glass and (b) silicon substrates coated with 100 nm Au. A comparison of TDTR sensitivity thermal conductivity for (c) glass and (d) silicon substrates coated with 100 nm Au assuming an interfacial contact resistance of $4 \cdot 10^{-8}$ m^2K/W.

for glass substrates, even large changes to the assumed value of contact resistance result in relatively small changes to the transient reflectivity curve. This additionally implies that, for a given contact resistance, the sensitivity of the shape of the transient reflectivity curve to thermal conductivity will increase as thermal conductivity decreases. This general behavior is shown in Figures 2c and 2d.

The sensitivity depends not only on the thermal properties of the sample, but also on the choice of transducer layer thickness. Analysis of model results shows that the maximum sensitivity of the measurement to interfacial resistance occurs at slightly different values of transducer thickness for different suspected values of interfacial resistance (Figure 3). Although the value of transducer thickness that maximizes sensitivity within a particular range of contact resistances is substrate dependent, the general trends shown in Figure 3 hold across a wide range of substrate thermal conductivities. In general, we expect sensitivity to contact resistance to be maximized by a thicker (thinner) transducer layer if the expected value of the contact resistance is larger (smaller). However, the dependence of ideal substrate thickness on substrate thermal conductivity is dwarfed by the more dramatic substrate thermal conductivity dependence of sensitivity to contact resistance, as will be shown below. We also note that, as seen in Figure 3, ns thermoreflectance measurements may require a larger transducer layer thickness than usually used either for fs or ps thermoreflectance measurements. Depending on the choice of transducer material, transducer layer thicknesses of several hundred nanometers may be needed to maximize the

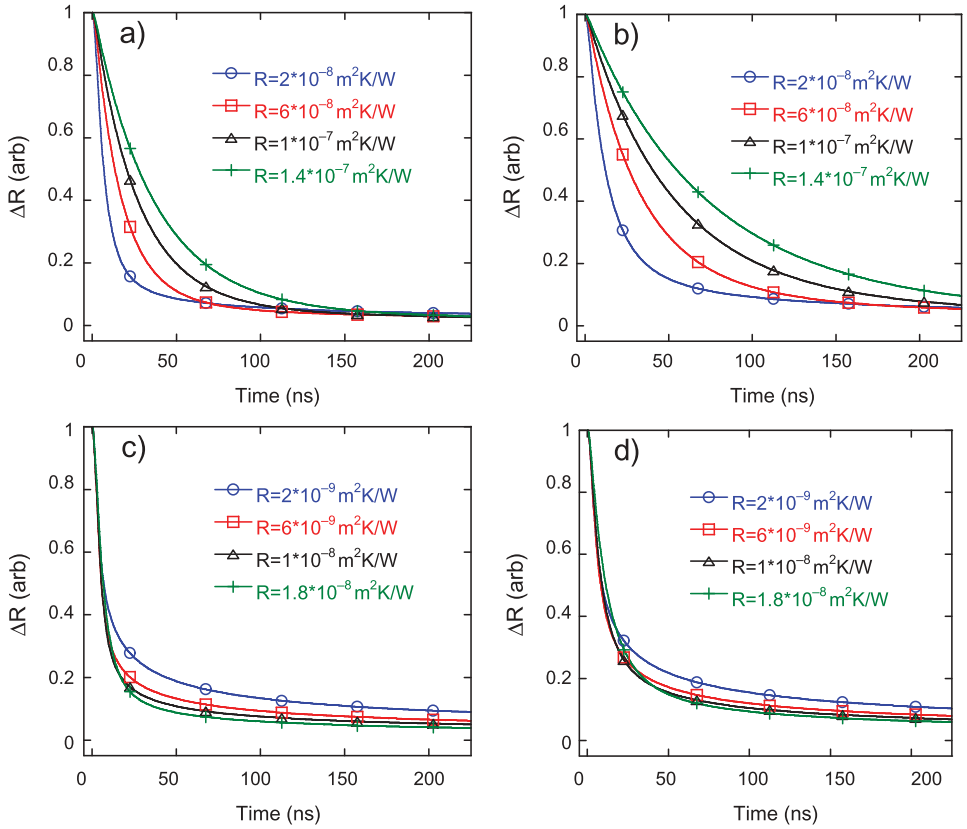

Figure 3 Comparison of TDTR sensitivity to interfacial contact resistance for (a,c) 100 nm and (b,d) 200 nm-thick Au on bulk silicon substrate. For possible contact resistance values greater than $2 \cdot 10^{-8}$ m^2K/W (a,b), the 200 nm-thick coating maximizes sensitivity to resistance, while for resistances less than $2 \cdot 10^{-8}$ m^2K/W (c,d), measurements of the 100 nm-thick coated sample are more sensitive.

sensitivity. On the other hand, these large thicknesses may be impractical owing to the possible introduction of inhomogeneities in the transducer layer during fabrication, and possible stress and hence adhesion problems caused by thick films. Nevertheless, sample preparation should be preceded by a detailed sensitivity analysis in order to determine the optimal transducer layer thickness. For cases where it is not possible to make, *a priori*, a precise estimation of the likely range of possible values of the interfacial resistance, it may be necessary to perform measurements on samples coated with several different thicknesses of transducer layer in order to ensure maximum sensitivity.

MEASUREMENT RESULTS AND DISCUSSION

To demonstrate the capability of the ns-TDTR method, we measure materials with relatively high thermal conductivity (Si and GaAs) and low thermal conductivity (glass), and the contact resistance between the gold coating and the substrate material. For practical reasons, we chose a thickness of gold coating of 100 nm.

The experimental ns-TDTR data for Si, GaAs, and fused quartz substrates are shown in Figure 4. Taking the substrate thermal conductivity as the literature value, we first show that it is possible to determine the metal-substrate thermal interface resistance. This is done via a least-squares algorithm in which the thermal resistance in the 1-D model is varied

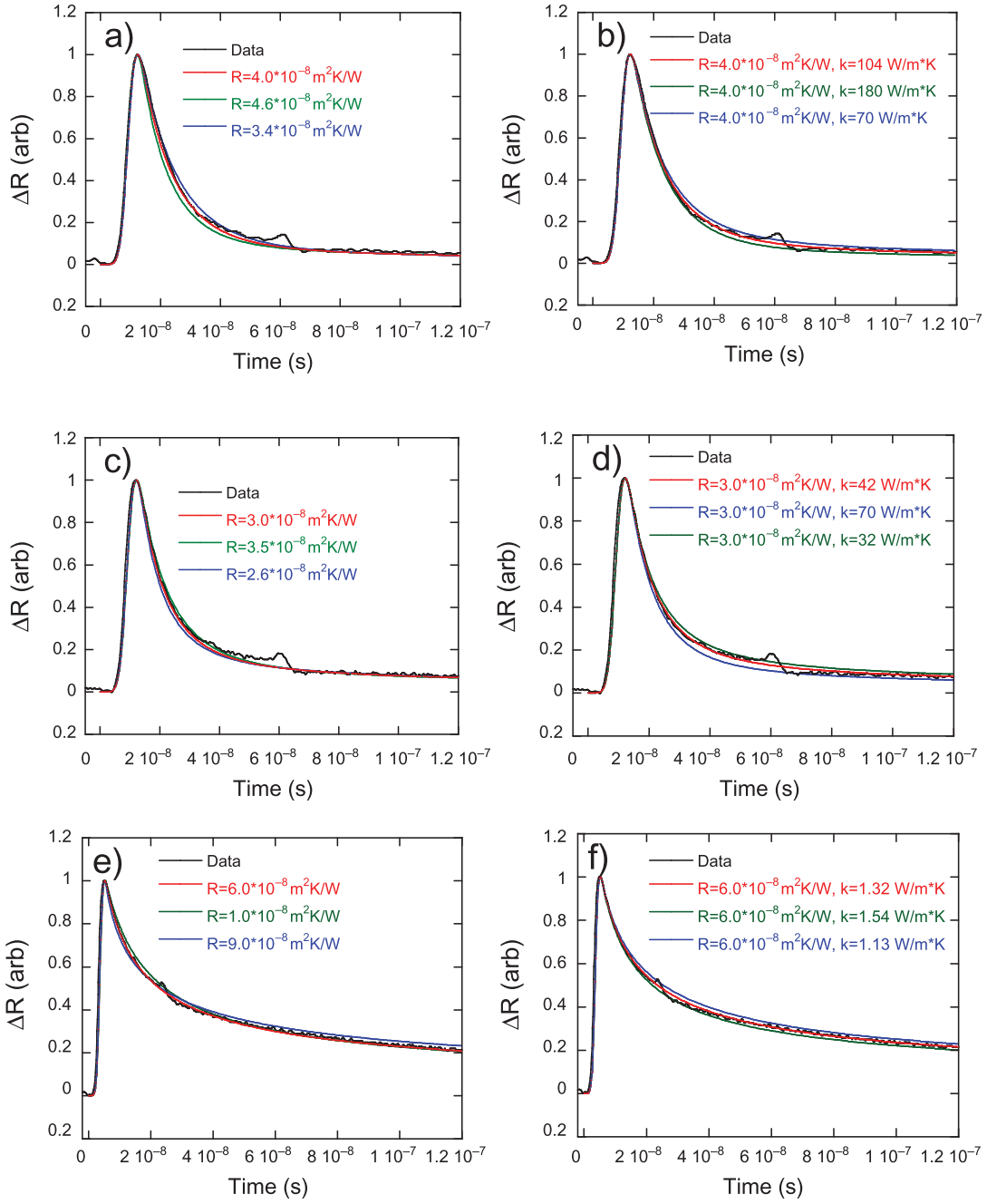

Figure 4 Illustration of the influences exerted by substrate thermal conductivity (left) and contact resistance (right) on measured transient reflectivity signals for Si (a-b), GaAs (c-d), and fused quartz (e-f) coated with 100 nm Au.

until a global minimum in the squared difference between the fit and model is reached. The contact resistance values determined are 4.0×10^{-8} m^{2}K/W, 3.0×10^{-8} m^{2}K/W, and 6.0×10^{-8} m^{2}K/W, respectively, for Si, GaAs, and fused quartz substrates. In order to characterize the uncertainty in the final results, the thermal resistance in the model is raised or lowered until the fit lies outside the noise level of the transient reflectivity data. These results are shown in Figure 4 (a, c, e). For example, the contact resistance for the silicon sample is well within the range between 3.4×10^{-8} m^{2}K/W and 4.0×10^{-8} m^{2}K/W.

We next consider the case (unlikely to be realized in practice) in which the interfacial thermal resistance is known, but the thermal conductivity of the substrate is not known. Here, we have chosen as the "known" value of the interfacial resistance those values that resulted in a best fit in Figure 4 (a, c, e). With contact resistance a known quantity, the least squares algorithm may be utilized to determine the value of thermal conductivity resulting in a best fit. The results are shown in Figure 4 (b, d, f).

From Figure 4, it is apparent that, the interfacial contact resistance primarily influences the first portion of the transient reflectivity curve while subsequent behavior is dominated by the thermal conductivity of the substrate. Because of this, it is possible to determine simultaneously both the conductivity of the substrate and the thermal contact resistance. When analyzing sensitivity to a parameter, x_o, which is either thermal conductivity or interface resistance, for a single material of interest, the sensitivity at any point of time during the thermal decay curve is, by convention, defined as $S_{x_o} = \frac{\partial(\ln \bar{T})}{\partial(\ln x_o)}$. For a broad set of materials and potential interface resistances and to further evaluate the sensitivity thermal conductivity or interface resistance across the widely varying material parameters, we define an integrated sensitivity parameter, $\tilde{S}_{x_o}$, by integrating the absolute difference in the logarithm of the normalized temperature decay curves, $\bar{T}(t)$, when the logarithm of the parameter x_o is changed by $+/-$ 10% of a nominal value across the time scale of interest, $t_i \leq t \leq t_f$:

$$\tilde{S}_{x_o} = \int_{t_i}^{t_f} \frac{\partial(\ln \bar{T})}{\partial(\ln x_o)}\, dt \approx \int_{t_i}^{t_f} \frac{\ln(\bar{T}_{1.1x_o}) - \ln(\bar{T}_{0.9x_o})}{\ln(1.1x_o) - \ln(0.9x_o)}\, dt. \tag{5}$$

Here we consider the sensitivity to substrate thermal conductivity and interface resistance across a large range of possible values, while keeping the geometry (100 nm of gold on a substrate) and the material properties for the gold transducer layer constant. The volumetric heat capacity (ρC_p) of the substrate was initially varied, but for this measurement configuration the normalized temperature decay is only sensitive to the effusivity of the substrate, $\epsilon = \left(k\rho C_p\right)^{\frac{1}{2}}$ [19]. Noting regions of high sensitivity to k compared to R_b'' in Figure 4, two time ranges are considered: (i) short times $0 \leq t \leq 50$ *ns* and (ii) long times $50 \leq t \leq 120$ *ns*. Figure 5 shows the sensitivity to thermal conductivity and sensitivity to interface resistance with varying the substrate material through the nominal effusivity and varying nominal contact resistance. It is seen in the short time regime, the measurement is more sensitive to interface resistance than to thermal conductivity for the range of expected effusivities and resistances. At long times, for low effusivities and the expected range of contact resistances (10^{-8} to 10^{-7} m^2 K/W), the measurement is more sensitive to thermal conductivity compared to contact resistance. But at long times with higher effusivities, the contact resistance and effusivity both impact the temperature decay curves and thus the sensitivity. Note that for other sample geometries, different sub-regions in time for the temperature decay curve may be more relevant, but this analysis illustrates the power of considering the time-dependent sensitivity.

The above may be seen as analogous to frequency domain [20] approaches to modeling heat transfer and its associated sensitivity to material properties: at short times, heat transfer is limited by conduction across the interface and as the heat propagates into the substrate the thermal conductivity plays a larger role. Correspondingly, considering the penetration depth in a frequency domain picture, the thermal response at higher frequencies

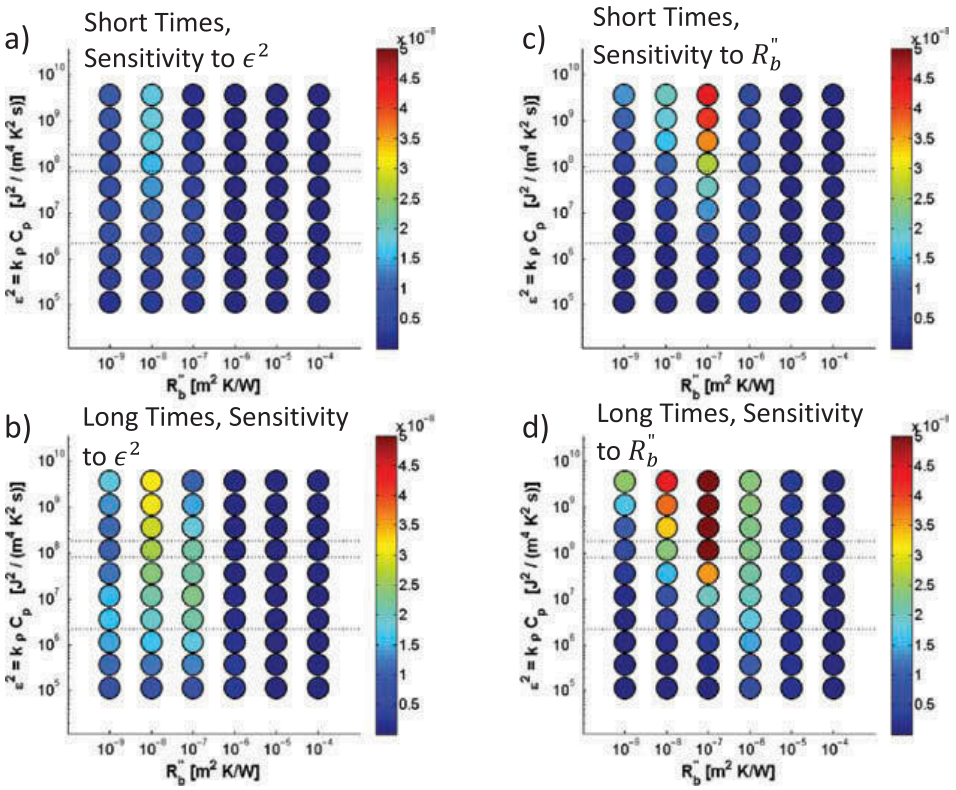

Figure 5 Sensitivity to (a-b) the square of substrate effusivity ($\epsilon^2 = k\rho C_p$) and (c-d) interface resistance at (a,c) short times ($t < 50$ ns) and (b,d) long times (50 ns $< t <$ 120 ns) as a function of interface resistance ($R_b^{"}$) and effusivity. Horizontal lines indicate the expected effusivity of Si, GaAs, and SiO_2. The expected range of thermal interface resistances is around 5×10^{-8} m^2 K/W. The sensitivity to the square of effusivity is exactly the sensitivity to thermal conductivity k if the volumetric heat capacity is fixed.

will be impacted more significantly by the contact resistance than that of lower frequency components with longer penetration depths into the substrate.

We next use an iterative procedure to determine both the interface resistance and substrate thermal conductivity. First, we choose a nominal value of substrate thermal conductivity and then use a least squares algorithm applied to the short times of the transient reflectivity curve to determine the interface resistance. The value of the contact resistance thus obtained is then incorporated into the model and the least squares algorithm applied to long times of the transient reflectivity curve (excluding the bump) to determine the thermal conductivity of the substrate. This process is then repeated until a two-parameter global minimum in the quality of the fit is reached. The uncertainty range of each thermal parameter can then be evaluated separately by increasing or decreasing a particular model parameter until the fit is made to lie just beyond the noise level of the transient reflectivity curve within the time region over which the parameter dominates the thermal transport.

Using the procedures described above, the results of fitting to obtain both thermal conductivity and interface contact resistance are shown in Figure 6. Such an approach yields a Si thermal conductivity in the range of 90–130 W/m*K, with a best-fit result of 109 W/m*K, and an interface contact resistance in the range of 3.5–5.0*10^{-8} m^{2}K/W. Similarly, the thermal conductivity of GaAs is in the range of 37–58 W/m*K with a best-fit result of 47 W/m*K, and the interface contact resistance in the range and 2.5–3.4*10^{-8}

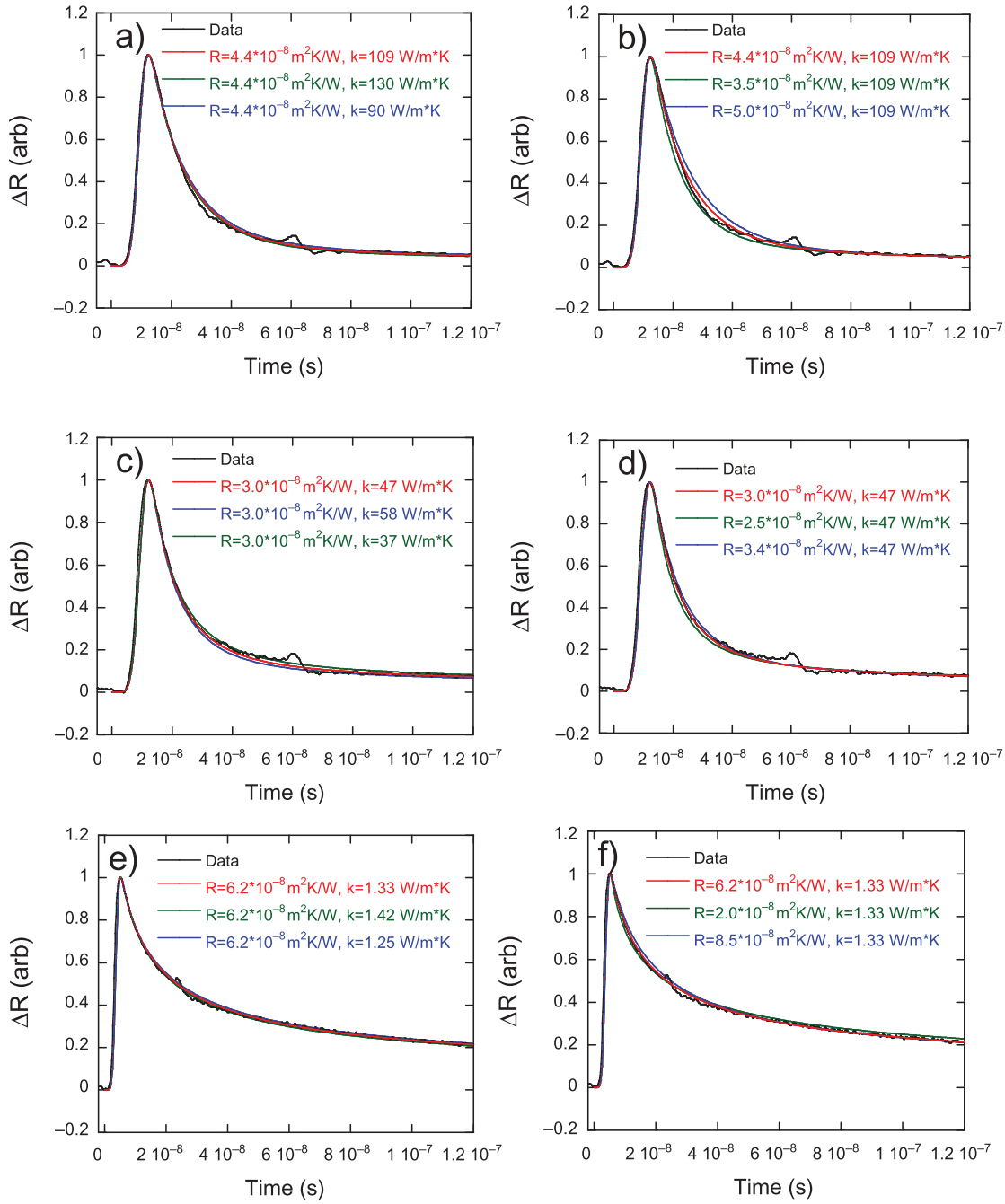

Figure 6 Illustration of global two-parameter best fit results and error bounds corresponding to a 1 standard deviation increase in the least squares error of the fit for Si (a-b), GaAs (c-d), and fused quartz coated with 100 nm Au.

m^2K/W. The thermal conductivity of fused quartz is measured to be in the range of 1.25–1.42 W/m*K with a best-fit result of 1.33 W/m*K. The interface contact resistance between the gold film and the fused quartz substrate is determined to be in the range of 2.0-8.5*10^{-8} m^2K/W with a best fit result of 6.2*10^{-8} m^2K/W. With the exception of Si, the textbook value of thermal conductivity lies within the error bounds obtained by model fits at the limit of the noise level. The range of contact resistances also agrees roughly with (although is somewhat higher than) those obtained in previous investigations

of interfacial thermal properties [16, 21-24]. For comparison, resistances of 2.0–8.5*10^{-8} m^2K/W correspond to conductances of 11.8–50.0 MW/m*K.

We note the value of the thermal conductivity obtained for Si is lower than textbook values. The thermal penetration depth $L_p = \left(2kt/\rho C_p\right)^{1/2}$ within the measurement time duration is roughly 4.5 μm. For silicon at room temperature, as much as 20% of thermal conductivity may be contributed by phonons with mean free path greater than 4.5 μm [25]. This may explain the low thermal conductivity values of bulk silicon obtained in our work.

The error bars provided above are comparable to those reported in some fs and literature [14, 26-27]. On the other hand, care must be taken in comparing uncertainties across experimental setups. In principle, both fs and ns approaches to thermoreflectance are capable of distinguishing any combination of thermal parameters provided the governing equations are not symmetric under an interchange of those parameters. For this reason, the error bars reported in any thermoreflectance measurement will be determined by the signal-to-noise ratio of the data. The error bars reported above may be improved through the addition of low noise detectors, increased averaging times, or the introduction of modulation techniques. Additionally, the combination of illumination wavelength and transducer material should, ideally, be chosen to maximize sensitivity of the reflectivity signal to temperature and, therefore, to the subsequent time-dependent thermal transport [28, 29].

CONCLUSION

Ns-TDTR provides a method of determining, from a single measurement, thermal properties including interface contact resistance. For bulk materials, interface and substrate thermal properties may be explored individually through the analysis of time-scale dependent influences each exerts on the resulting transient reflectivity curve. Generally, sensitivity of the measurement to a particular thermal property of interest will be greater if that property dominates the cooling of the metal transducer layer. Thus, if cooling of the transducer layer is limited by thermal contact resistance rather than the thermal properties of the substrate, the method will be relatively more sensitive to contact resistance than substrate thermal conductivity, and vice versa. As a specific application, for low thermal conductivity materials such as thermoelectric materials, their thermal conductivity can be relatively accurately determined using this method. We also show that it is possible to determine iteratively both contact resistance and thermal conductivity from a single measurement, with the experimental uncertainly determined by the experimental noise.

FUNDING

Partial support to this work by the DARPA MESO program (Grant N66001-11-1-4107), the National Science Foundation, and DOE DE-FC26-04NT42278 are gratefully acknowledged.

REFERENCES

1. D.G. Cahill, W.K. Ford, K.E. Goodson, G.D. Mahan, A. Majumdar, H.J. Maris, R. Merlin, S.R. Phillpot, Nanoscale Thermal Transport, *Journal of Applied Physics*, Vol. 93, pp. 793–818, 2003.

2. D.G. Cahill, Thermal Conductivity Measurement from 30 to 750 K: the 3ω Method, *Review of Scientific Instruments*, Vol. 61, pp. 802–808, 1990.
3. F. Volklein, Thermal Condctivity and Diffusivity of a Thin Film SiO_2-Si_3N_4 Sandwich System, *Thin Solid Films*, Vol. 188, pp. 27–33, 1990.
4. M. Okuda and S. Ohkubo, A Novel Method for Measuring the Thermal Conductivity of Submicrometer Thick Dielectric Films, *Thin Solid Films*, Vol. 213, pp. 176–181, 1992.
5. S. Perichon, V. Lysenko, B. Remaki, D. Barbier, B. Champagnon, Measurement of Porous Silicon Thermal Conductivity by Micro-Raman Scattering, *Journal of Applied Physics*, Vol. 86, pp. 4700–4702, 1999.
6. Z. Luo, H. Liu, B.T. Spann, Y. Feng, P. Ye, Y.P. Chen, X. Xu, Measurement of In-Plane Thermal Conductivity of Ultrathin Films Using Micro-Raman Spectroscopy, *Nanoscale and Microscale Thermophysical Engineering*, Vol. 18, pp. 183–193, 2014.
7. X. Wang, H. Hu, X. Xu, Photo-Acoustic Measurement of Thermal Conductivity of Thin Films and Bulk Materials, *Journal of Heat Transfer*, Vol. 123, pp. 138–144, 2001.
8. C.A. Paddock and G.L. Eesley, Transient Thermoreflectance from Thin Metal Films, *Journal of Applied Physics*, Vol. 60, pp. 285–290, 1986.
9. M. Omini, A. Sparavigna, A. Strigazzi, Dilatometric determination of Thermal Diffusivity in Low Conducting Materials, *Measurement Science Technology*, Vol. 1, pp. 166–171, 1990.
10. W.J. Parker, R.J. Jenkins, C.P. Butler, G.L. Abbott, Method of Determining Thermal Diffusivity, Heat Capacity and Thermal Conductivity, *Journal of Applied Physics*, Vol. 32, pp. 1679–1684, 1961.
11. B.C. Daly, H.J. Maris, W.K. Ford, G.K. Antonelli, L. Wong, E. Andideh, Optical Pump and Probe Measurement of the Thermal Conductivity of Low-*k* Dielectric Thin Films, *Journal of Applied Physics*, Vol. 92, pp. 6005–6009, 2002.
12. C.J. Morath, H.J. Maris, J.J. Cuomo, D.L. Pappas, A. Grill, V.V. Patel, J.P. Doyle, K.L. Saenger, Picosecond Optical Studies of Amorphous Diamond and Diamondlike Carbon: Thermal Conductivity and Longitudinal Sound Velocity, *Journal of Applied Physics*, Vol. 76, pp. 2636–2640, 1994.
13. A.J. Schmidt, R. Cheaito, M. Chiesa, A Frequency-Domain Thermoreflectance Method for the Characterization of Thermal Properties, *Review of Scientific Instruments*, Vol. 80, p. 094901, 2009.
14. J.A. Malen, K. Baheti, T. Tong, Y. Zhao, J.A. Hudgings, A. Majumdar, Optical Measurement of Thermal Conductivity Using Fiber Aligned Frequency Domain Thermoreflectance, *Journal of Heat Transfer*, Vol. 133, p. 081601, 2011
15. D.G. Cahill, Analysis of Heat Flow in Layered Structures for Time-Domain Thermoreflectance, *Review of Scientific Instruments*, Vol. 75, pp. 5119–5122, 2004.
16. A.N. Smith, J.L. Hostetler, P.M. Norris, Thermal Boundary Resistance Measurements Using a Transient Thermoreflectance Technique, *Microscale Thermophysical Engineering*, Vol. 4, pp. 51–60, 2000.
17. S. Huxtable, D.G. Cahill, V. Fauconnier, J.O. White, J.C. Zhao, Thermal Conductivity Imaging at Micro-Scale Resolution for Combinatorial Studies of Materials, *Nature Materials*, Vol. 3, pp. 298–301, 2004.
18. L. Guo, S.L. Hodson, T.S. Fisher, X. Xu, Heat Transfer Across Metal-Dielectric Interfaces During Ultrafast-Laser Heating, *Journal of Heat Transfer*, Vol. 134, p. 042402, 2012.
19. J.L. Battalglia and A. Kusiak, Thermal Diffusivity of Thin Layers Using Time-Domain Thermoreflectance, *Physical Review B*, Vol. 76, p. 184110, 2007.
20. K.C. Collins, A.A. Mazney, J. Cuffe, K.A. Nelson, G. Chen, Examining Thermal Transport Through a Frequency-Domain Representation of Time-Domain Thermoreflectance Data, *Review of Scientific Instruments*, Vol. 85, 124903, 2014.
21. E. Bozorg-Grayeli, J.P. Reifenberg, K.W. Chang, M. Panzer, J.A. Rowlette, K.E. Goodson, Temperature-Dependent Thermal Properties of Phase-Change Memory Electrode Materials, *Electron Device Letters*, Vol. 32, pp. 1281–1283, 2011.

22. R.J. Stevens, A.N. Smith, P.M. Norris, Measurement of Thermal Boundary Conductance of a Series of Metal-Dielectric Interfaces by the Transient Thermoreflectance Technique, *Journal of Heat Transfer*, Vol. 127, pp. 315–322, 2005.
23. R.M. Cotescu, M.A. Wall, D.G. Cahill, Thermal Conductance of Epitaxial Interfaces, *Physical Review B*, Vol. 67, p. 054302, 2003.
24. R.J. Stoner and H.J. Maris, Kapitza Conductance and Heat Flow Between Solids at Temperatures From 50 to 300 K, *Physical Review B*, Vol. 48, pp. 16373–16387, 1993.
25. K.T. Regner, D.P. Sellan, Z. Su, C.H. Amon, A.J.H McGaughy, J.A. Malen, Broadband Phonon Mean Free Path Contributions to Thermal Conductivity Measured Using Frequency Domain Thermoreflectance, *Nature Communications*, Vol. 4, 1640, 2013.
26. Y.K. Koh, M.H. Bae, D.G. Cahill, E. Pop, Heat Conduction Across Monlayer and Few-layer Graphenes, *Nano Letters*, Vol. 10, pp. 4363–4368, 2010.
27. C. Chiritescu, D.G. Cahill, N. Nguyen, D. Johnson, A. Bodapati, P. Keblinski, P. Zschack, Ultralow Thermal Conductivity in Disordered, Layered WSe_2 Crystals, *Science*, Vol. 315, pp. 351–353, 2007.
28. Y. Wang, J.Y. Park, Y.K. Koh, D.G. Cahill, Thermoreflectance of Metal Transducers for Time-Domain Thermoreflectance, *Journal of Applied Physics*, Vol. 108, 043507, 2010.
29. R.B. Wilson, B.A. Apgar, L.W. Martin, D.G. Cahill, Thermoreflectance of Metal Transducers for Optical Pump-Probe Studies of Thermal Properties, *Optics Express*, Vol. 20, 28829, 2012.